

SYNTHESIS, SPECTROSCOPIC CHARACTERIZATIONS AND BIOLOGICAL STUDIES ON GOLD(III), RUTHENIUM(III) AND IRIIDIUM(III) COMPLEXES OF TRIMETHOPRIM ANTIBIOTIC DRUG

Abeer A. El-Habeeb¹ and Moamen S. Refat^{2*}

¹Department of Chemistry, College of Science, Princess Nourah bint Abdulrahman University, P.O. Box 84428, Riyadh 11671, Saudi Arabia

²Department of Chemistry, College of Science, Taif University, P.O. Box 11099, Taif 21944, Saudi Arabia

(Received October 13, 2023; Revised January 30, 2024; Accepted February 2, 2024)

ABSTRACT. Ruthenium(III), gold(III), and iridium(III) trimethoprim drug (TMP) complexes were synthesized and analysed via microanalytical approach (C, H, N analysis), magnetic, molar conductance, and FTIR, ¹H NMR, XRD, and UV-Vis spectroscopy. Through two nitrogen atoms of –NH₂ amino groups, the TMP drug coordinated as a bidentate ligand towards the corresponding three metal ions. The geometrical structure of the compounds ruthenium(III), gold(III), and iridium(III) is octahedral and consists of two TMP molecules, two coordinated chlorine atoms, and one uncoordinated chlorine atom. The antibacterial properties of TMP complexes have been investigated through the use of many bacterial species, including *Pseudomonas aeruginosa*, *Bacillus subtilis*, *Staphylococcus aureus*, and *Escherichia coli*. Additionally, the generated complexes' anticancer properties against HepG-2 (human hepatocellular carcinoma) and MCF-7 (human breast cancer cell line) have been assessed. In contrast to those of clinically used antibiotics, the inhibition zone of ruthenium and iridium(III) complexes was in the low efficiency range, and the antibacterial activity of gold(III) complexes was moderate. This article discusses the possibilities and prospects for this family of metallodrugs as antibacterial or anticancer medicines.

KEY WORDS: Trimethoprim drug, Chelation, Gold, TEM, XRD, FTIR

INTRODUCTION

It is commonly known that trimethoprim (2,4-diamino-5-(3,4,5-trimethoxy benzyl) pyrimidine, TMP) inhibits the enzyme dihydrofolate reductase (DHFR). It has antiparasitic properties as well as being a member of the synthetic antibacterial agent class known as diaminopyrimidines [1]. It works well against illnesses brought on by both Gram-positive and Gram-negative bacteria [2], as well as the majority of common bacterial species [3]. On the other hand, simple urinary tract infections can be prevented and treated with trimethoprim alone [4]. It is well known that the majority of these compounds are vulnerable to interference by oxygen, nitrogen, or sulphur atoms included in the medication formulations when haemoglobin in the blood is involved [5]. Those who take significant doses of these antibiotics experience a decrease in the amount of iron in their bodies due to the binding property [6], preventing its association with haemoglobin. As a result, researchers started to consider and look for new medications to treat drug-resistant illnesses. On the other hand, these medications don't interact with haemoglobin in cases where another binding (such as metal ions) has blocked their active sites. Metal–drug complexes have drawn a lot of interest and produced a number of innovative and useful medications. Numerous domains are the subject of ongoing research [7-17], when found in bodily fluids or tissue cells, many metal complexes have greater action against a variety of microorganisms, even those that have a high level of resistance to the antibiotic itself. For example, it has been discovered that the metal complexes of sulfa medications are more bacteriostatic than the antibiotic itself [18-20]. Trimethoprim organometallic compounds play a significant role in coordination chemistry. With

*Corresponding author. E-mail: moamen@tu.edu.sa ; msrefat@yahoo.com

This work is licensed under the Creative Commons Attribution 4.0 International License

the majority of transition metals, it forms stable complexes and exhibits stronger antibacterial and antimicrobial properties. Trimethoprim interacts as a monodentate ligand when it forms complexes with transition metal ions, such as those with Cu(II), Zn(II), Pt(II), Ru(II), Fe(III), Cd(III), Co(III), and Co(II) [21, 22]. Trimethoprim also forms square planar, tetrahedral, and octahedral geometries [20-22]. Recent years have seen a considerable increase in interest in trimethoprim-transition metal complexes because of their remarkable biological qualities, stability, and simplicity of modification. In light of this, our goals for this work are to: i) construct the Au(III), Ru(III), and Ir(III) complexes using the antifolate-trimethoprim medication; ii) characterize the synthesis complexes; and iii) investigate the antibacterial and anticancer properties of the generated complexes.

EXPERIMENTAL

Chemicals

Without additional purification, trimethoprim medication, gold(III) chloride, iridium(III) chloride, and ruthenium(III) chloride hydrate salts were utilized in the synthesis after being obtained from Sigma-Aldrich Chemical Company, USA.

Instruments

The types of analyses and models that go along with them are as follows:

Analytical type	Specifications
Elemental analyses	Perkin Elmer CHN 2400
Melting points	Stuart Melting Point Apparatus
Conductance	Jenway 4010 conductivity meter
FTIR spectra	Bruker FTIR Spectrophotometer
Electronic spectra	UV2 Unicam UV/Vis Spectrophotometer
Magnetic moment	Magnetic Susceptibility Balance
¹ H NMR spectra	500 MHz Jeol Jnm Eca 500 NMR Spectrometer
Thermo gravimetric	TG/DTG-50H, Shimadzu thermo-gravimetric analyzer
XRD spectra	X 'Pert PRO PANanalytical, with copper target
SEM	Jeol Jem-1200 EX II at an acceleration voltage of 25 kV
TEM	Jeol, 100s microscope

Synthesis

To generate ruthenium, gold, and iridium(III) trimethoprim complexes, 1.0 mmol each of RuCl₃ (0.208 g), AuCl₃ (0.304), and IrCl₃.xH₂O (0.299 g) were mixed with 2.0 mmol TMP (0.581 g) in 30 mL of methanol. After the mixtures were refluxed for around four hours until colored precipitates started to form, the solid products were filtered out and repeatedly washed with small volumes of methanol. In a vacuum desiccator set over anhydrous CaCl₂, the solid precipitates were dried and sealed.

RESULTS AND DISCUSSION

Elemental analysis and physical measurements

The yields of the solid products of the ruthenium(III), gold(III), and iridium(III) TMP complexes range from 75-79%. The produced complexes are soluble in organic solvents like DMSO and DMF but insoluble in water and most other organic solvents. Three TMP complexes that were synthesized have a melting point of about >300 °C. It is supported by the lack of impurities that

the solid complexes have sharp melting points. The theoretical data, as shown in Table 1, is in good agreement with the microanalysis (C, H, N, and metal percentages) of the experimental results. Figure 1 shows the chemical formula $[M(\text{TMP})_2(\text{Cl})_2]\cdot\text{Cl}$, along with the hypothesized structures of 1:2 (M:TMP) Ru(III), Au(III), and Ir(III)-TMP complexes. The Ru(III), Au(III), and Ir(III)-TMP complexes synthesized at a 10^{-3} M concentration and dispersed in dimethyl sulfoxide (DMSO) solvent exhibit molar conductance's of $\Lambda_m = 37$, 42, and 39 $\text{ohm}^{-1}\cdot\text{cm}^2\cdot\text{mol}^{-1}$, respectively. The electrolytic property of all three TMP complexes was corroborated by the obtained data [23]. The development of novel compositions was confirmed by the appearance of colored complexes.

Table 1. Microanalysis and physical data of Ru, Au, and Ir(III)-TMP complexes.

Complex	Color	Conductance/ ($\text{ohm}^{-1}\cdot\text{cm}^2\cdot\text{mol}^{-1}$)	Element	Calc./%	Found/%
Ru(III)	Greenish black	37	C	42.64	42.44
			H	4.57	4.51
			N	14.21	14.10
			Ru	12.82	12.77
Au(III)	Orange	42	C	38.01	38.00
			H	4.07	4.04
			N	12.67	12.55
			Au	22.28	22.16
Ir(III)	Black	39	C	38.22	38.17
			H	4.09	4.07
			N	12.74	12.65
			Ir	21.86	21.79

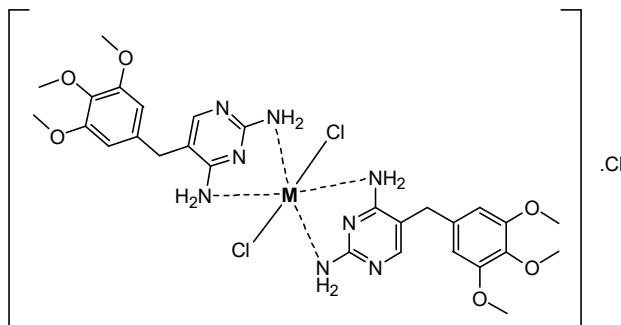


Figure 1. Suggested structures of Ru(III), Au(III), and Ir(III)-TMP complexes.

FTIR spectra

The infrared spectra of the trimethoprim free ligand, Ru(III), Au(III), and Ir(III) complexes are shown in Figure 2, and their assignments are listed in Table 2. Through pyrimidine nitrogen atoms ($-\text{NH}_2$ and $-\text{C}=\text{N}$ groups) and oxygen of methoxyl groups, the trimethoprim free ligand possesses an oxygen and nitrogen donating atom. $\nu_{\text{as}}(\text{NH}_2)$, $\nu_{\text{s}}(\text{NH}_2)$, $\nu(\text{C}=\text{N})$, $\nu(\text{C}=\text{C})$ of the pyrimidine and trimethoxy moieties give rise to several distinctive groups in trimethoprim-free medication, with stretching frequencies at 3470, 3319, 1635 and 1594 cm^{-1} . After complexation, the pyrimidine ring's vibration bands $\nu_{\text{as}}(\text{NH}_2)$, $\nu_{\text{s}}(\text{NH}_2)$ and $\nu(\text{C}=\text{N})$ shift to lower/higher wavenumbers and exhibit within the range of $3429\text{--}3404\text{ cm}^{-1}$, $3333\text{--}3318\text{ cm}^{-1}$, and $1659\text{--}1638\text{ cm}^{-1}$, respectively.

These results supported the coordinated movement of the amino group's nitrogen atoms towards central metal ions, which the stretching vibration of $\nu(\text{C}=\text{N})$ of pyrimidine ring is set not changed, because of not involved in the coordination process [24, 25]. The existence of additional frequencies in the complexes' spectra at the 529–427 cm^{-1} region is ascribed to $\nu(\text{M}-\text{N})$ and [25]. The TMP coupled to respected metal ions as a bi-dentate ligand through the nitrogen atoms of the NH_2 amino groups, as proven by the infrared assignments [26].

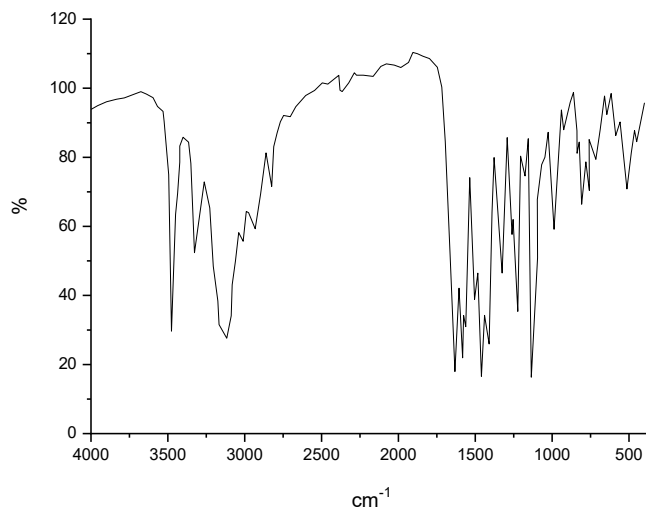


Figure 2A. FTIR spectrum of TMP free drug.

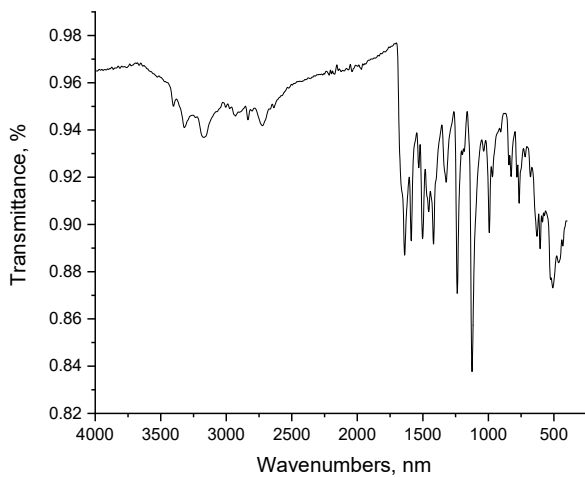


Figure 2B. FTIR spectrum of Ru(III)-TMP complex.

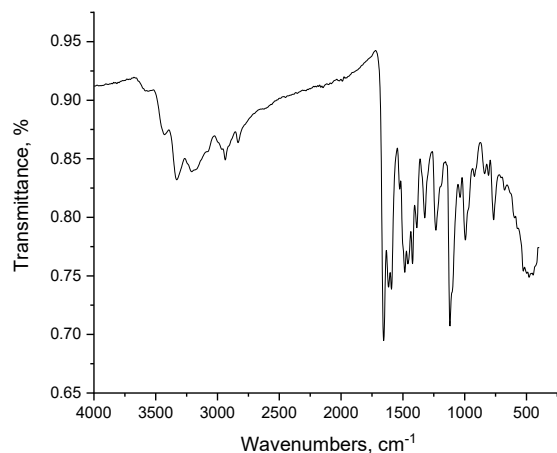


Figure 2C. FTIR spectrum of Au(III)-TMP complex.

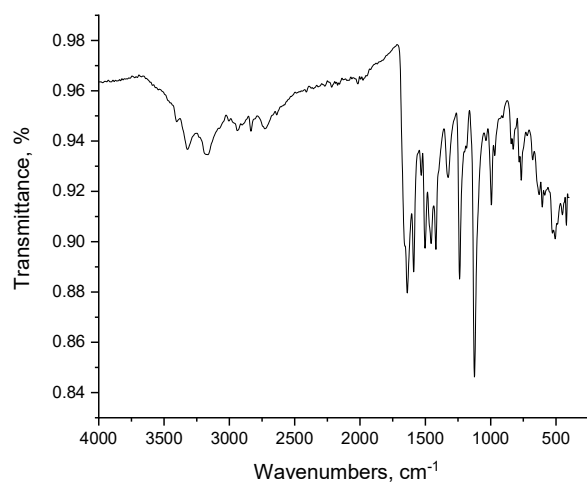


Figure 2D. FTIR spectrum of Ir(III)-TMP complex.

Table 2. Infrared spectral data (cm^{-1}) of TMP and Ru, Au, and Ir(III)-TMP complexes.

Compounds	Frequencies, cm^{-1}				
	$\nu_{\text{as}}(\text{NH})$	$\nu_{\text{s}}(\text{NH})$	$\nu(\text{C}=\text{N})$	$\nu(\text{C}=\text{C})$	$\nu(\text{M}-\text{N})$
TMP	3470	3319	1635	1594	-
Ru(III)	3404	3318	1638	1593	508, 463, 427
Au(III)	3429	3333	1659	1593	529, 483, 443
Ir(III)	3408	3322	1638	1593	529, 508, 448

Electronic spectra and magnetic susceptibility

In order to obtain electronic UV-Vis spectra in the 800-200 nm range, the Ru(III), Au(III), and Ir(III)-TMP complexes with 10^{-3} M in DMSO solvent were scanned. Table 3 lists the assignments

of electronic peaks. Three electronic transitions are visible in the Ru(III) complex at 24390 cm^{-1} , 30488 cm^{-1} , and 36496 cm^{-1} . It is possible to attribute these transitions to ${}^2T_{2g} \rightarrow {}^4T_{1g}$ (v1), ${}^2T_{2g} \rightarrow {}^4T_{2g}$ (v2), and ${}^2T_{2g} \rightarrow {}^2A_{2g}$ (v3). Calculations are made for the ligand field parameters (10 Dq), the Racah interelectronic repulsion parameters (B and C), and the nephelauxetic parameter ($\beta = B/B'$, where $B' = 630 \text{ cm}^{-1}$). The observation of a single unpaired electron in an octahedral environment for the Ru(III) ion in a low spin $4d^5$ configuration is supported by the magnetic moment of 2.11 B.M. of the ruthenium(III) complex [27-33].

Observing all of the anticipated bands may be impossible due to interference caused by charge-transfer transitions in the electronic spectra of the gold(III) complex [32, 33]. Metal ligand charge transfer ($M \rightarrow L_{CT}$) and the d-d transition band can be used to explain the distinct bands at 33898 cm^{-1} and 28409 cm^{-1} . The other weak band at 25000 cm^{-1} is caused by the combination of d-d transition bands and $N \rightarrow Au(III)$ metal charge transfer ($L\pi \rightarrow Au_{CT}$). The geometry of the gold(III) complex must be octahedral as it displays diamagnetic properties. After complexation, a decrease in frequency is caused by the interaction of the amino group nitrogen atom with the Au(III) ion.

The iridium(III) complex has a diamagnetic property. The iridium(III) complex's UV-Vis spectrum has bands at 30395 cm^{-1} and 35714 cm^{-1} . These two bands were inferred from the ground state ${}^1A_{1g}$. Regarding the two spin-allowed transitions, ${}^1A_{1g} \rightarrow {}^1T_{1g}$ (v1) and ${}^1A_{1g} \rightarrow {}^1T_{2g}$ (v2), they were discovered within the expected ranges [27-31]. According to the octahedral geometry for iridium(III) complexes described in the literature [33], the ratio v2/v1 in the Ir(III) complex is 1.1750. The ${}^1A_{1g} \rightarrow {}^1T_{1g}$ (v1) and ${}^1A_{1g} \rightarrow {}^1T_{2g}$ (v2) transitions have been used to calculate the ligand field parameters 10Dq and nephelauxetic (B) [32,33]. The resultant values of the v2/v1, 10Dq, B, C, and β parameters agree with those of other iridium(III) complexes from previous studies [32, 33]. B value in the Ir(III) complexes indicates a significant covalency overlap in the metal ligand σ -bond and corresponds to about 49.70% of the free iridium ion (660 cm^{-1}).

Table 3. Electronic spectral bands (cm^{-1}) and ligand field parameters of Ru^{3+} , Au^{3+} and Ir^{3+} -TMP complexes.

Complex	v2/v1	10 Dq (cm^{-1})	B (cm^{-1})	C (cm^{-1})	β
Ru(III)	1.2500	41292	762	3273	1.209
Au(III)	-	-	-	-	-
Ir(III)	1.1750	31725	332	1330	0.5030

¹H NMR spectrum

The ¹H NMR spectrum data of the trimethoprim gold(III) complex in d_6 -DMSO refer to the present of distinguish proton signals as compared to that of the free trimethoprim ligand (δ , ppm) = 3.533 (2H, CH₂), 3.620-3.725 (9H, 3OCH₃), 6.559 (2H, trimethoxy moiety), 7.529 (1H, pyrimidine moiety), 6.14 and 7.529 (4H, NH₂ pyrimidine moiety) [34]. The proton NMR of [Au(TMP)₂(Cl)₂].Cl showed two major peaks at the aromatic region for three protons at δ (ppm) (7.395-7.528 and 7.598-7.760) and 8.295-8.382 ppm assigned to (2H, trimethoxy moiety) and (1H, pyrimidine moiety), respectively. The two protons of the methylene group are located at δ (ppm) = 3.578-3.615 (2H, CH₂) and in case of the protons of trimethoxy group can be observed as a peaks at δ (ppm) 3.709-3.815 (9H, 3OCH₃) regarding for nine protons. In [Au(TMP)₂(Cl)₂].Cl four major peaks can also be observed in the NH₂ region which were successfully assigned at δ (ppm) = 6.582, 6.608, 6.989, and 6.999 ascribed to (4H, NH₂ pyrimidine moiety) for two trimethoprim moiety. The coordination of the gold(III) metal ions can be seen from the downfield shift of the proton NMR signals assigned in this spectrum (Figure 3).

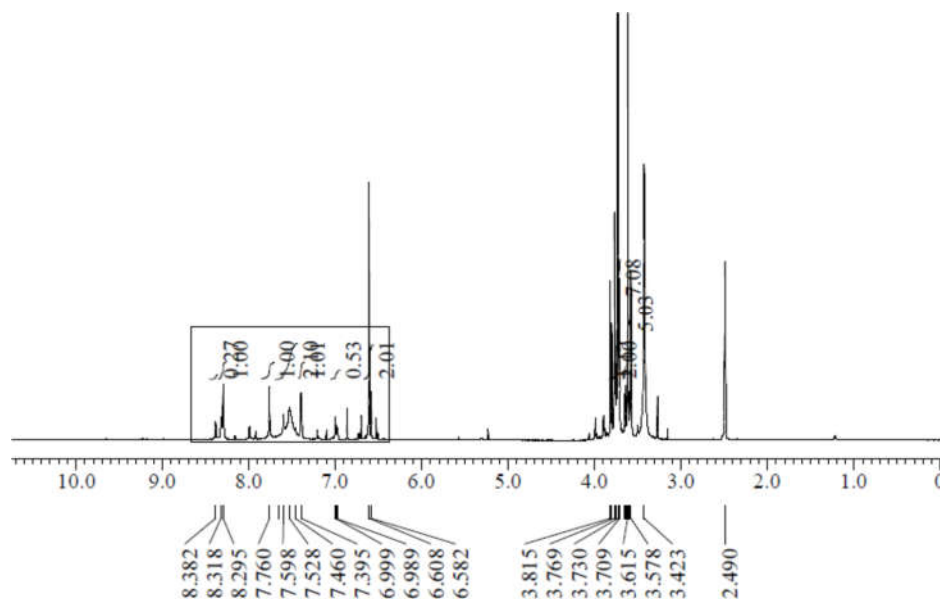


Figure 3. ^1H NMR spectrum of Au(III)-TMP complex.

Differential scanning calorimeter

DSC thermograms have shown an endothermic peak of trimethoprim pure drug at 203 °C [35], which corresponded to its melting point. DSC thermograms (Figures 4A-C and Table 4) of trimethoprim–Ru(III), trimethoprim–Au(III) and trimethoprim–Ir(III) metal complex showed endothermic peaks at (277, 320, 388 and 751°C), (169, 296, 344 and 495°C) and (285, 394, 487 and 561°C), respectively). The results of the thermograms obtained from DSC of trimethoprim–Ru(III), trimethoprim–Au(III) and trimethoprim–Ir(III) metal complexes revealed the interaction between the drug and metals. The thermogravimetric studies of all the trimethoprim–Ru(III), trimethoprim–Au(III) and trimethoprim–Ir(III) complexes were carried out under nitrogen atmosphere at a heating rate of 15 °C/min per minute. The thermal decomposition of the complexes proceeds in three-to-four stages. The trimethoprim–Ru(III), trimethoprim–Au(III) and trimethoprim–Ir(III) complexes are thermally stable up to 177, 140 and 197 °C, respectively. This table agreed with the elemental analysis of Table 1. The first stage of decomposition corresponds to endothermic decomposition of complexes by the loss of chlorine atoms occurs in the temperature range 177–308, 140–210, and 197–385 °C, respectively. The second decomposition with endothermic peak by the loss of two TMP ligand moieties occurs in the temperature range at 308–800, 210–800 and 385–800 °C, respectively. The solid residues above 540, 650 and 557 °C were identified as RuO₂ oxide, Au metal and IrO₂ oxide, respectively. In all the complexes, the final products are metal-to-metal oxides.

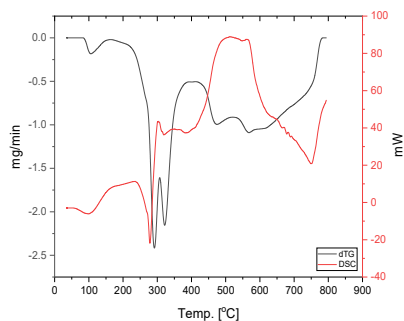
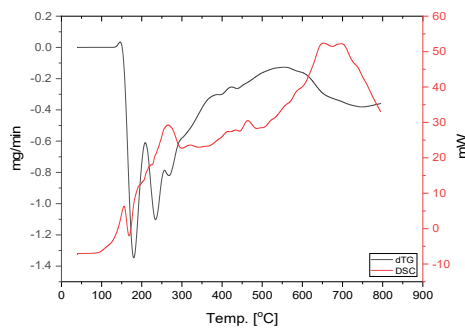
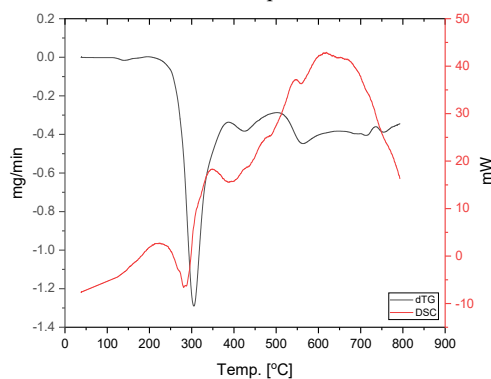
Figure 4A. DSC thermogram of Ru³⁺-TMP complex.Figure 4B. DSC thermogram of Au³⁺-TMP complex.Figure 4C. DSC thermogram of Ir³⁺-TMP complex.

Table 4. Thermal analytical data of the trimethoprim metal complexes.

Complex	Stage	Temp. range/ °C	Assignment	Mass loss/ %	Residue
Ru(III)	1 st	177-308	3Cl	13.51	RuO ₂
	2 nd	308-420			
	3 rd	420-541	2TMP	73.68	
	4 th	541-800			
Au(III)	1 st	140-210	3Cl	12.05	Au metal
	2 nd	210-378	2TMP	65.69	
	3 rd	378-650			
	4 th	650-800			
Ir(III)	1 st	197-385	3Cl	12.11	IrO ₂
	2 nd	385-557	2TMP	66.04	
	3 rd	557-793			

Scanning and transmission electron microscopy

Three distinct magnifications (3–50 μm) were used to capture the morphological SEM micrographs of the trimethoprim–Ru(III), trimethoprim–Au(III), and trimethoprim–Ir(III) metal complexes. While $[\text{Au}(\text{TMP})_2(\text{Cl})_2]\cdot\text{Cl}$ displayed a structure resembling little stones, the $[\text{Ru}(\text{TMP})_2(\text{Cl})_2]\cdot\text{Cl}$ complex displayed condensed slices, and $[\text{Ir}(\text{TMP})_2(\text{Cl})_2]\cdot\text{Cl}$ displayed a

well-homogeneous structure with huge stone structures (Figure 1S, supplementary material). The structural alteration and the development of new complexes are evident in the SEM micrographs of the trimethoprim metal complexes, trimethoprim–Ru(III), trimethoprim–Au(III), and trimethoprim–Ir(III).

Trimethoprim–Ru(III), trimethoprim–Au(III), and trimethoprim–Ir(III) complexes nanoparticles are amorphous aggregates, as demonstrated by the TEM image (Figure 2S, supplementary material). Based on TEM images, the size of the complexes' nanoparticles, $[\text{Ru}(\text{TMP})_2(\text{Cl})_2]\cdot\text{Cl}$, $[\text{Au}(\text{TMP})_2(\text{Cl})_2]\cdot\text{Cl}$, and $[\text{Ir}(\text{TMP})_2(\text{Cl})_2]\cdot\text{Cl}$, are determined to be between 30–36 nm.

Powder XRD studies of trimethoprim metal complexes

In qualitative terms, the degree of crystallinity is explained by the XRD patterns. According to Figure 5A–C, the diffractograms for $[\text{Ru}(\text{TMP})_2(\text{Cl})_2]\cdot\text{Cl}$, $[\text{Au}(\text{TMP})_2(\text{Cl})_2]\cdot\text{Cl}$ and $[\text{Ir}(\text{TMP})_2(\text{Cl})_2]\cdot\text{Cl}$ complexes shows values ranging from 2 to 70° (2θ). The graph compares all of the peaks indexed 2θ values. When the values are compared, they show that the values of 2θ and d values match well together [36].

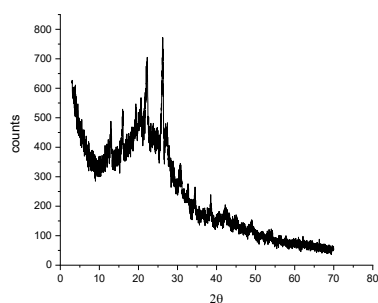


Figure 5A. XRD spectrum of Ru(III)-TMP complex.

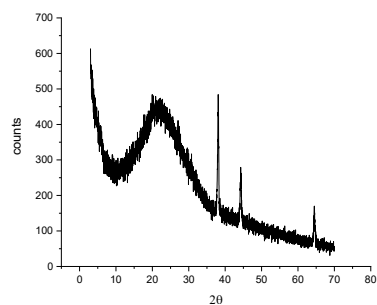


Figure 5B. XRD spectrum of Au(III)-TMP complex.

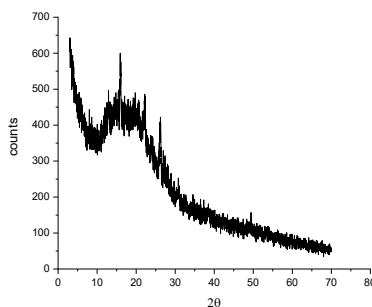


Figure 5C. XRD spectrum of Ir(III)-TMP complex.

As indicated by Figure 5A, the diffraction peaks at 2θ values 38, 42, 45, 56, and 66° were indexed as 100, 002, 101, 102, and 110, respectively. Using X-ray diffraction, the synthesis of the $[\text{Au}(\text{TMP})_2(\text{Cl})_2]\cdot\text{Cl}$ metal complex was verified. As seen in Figure 5B, the diffractogram of the trimethoprim–Au(III) complex shows peaks at 2θ values of 38, 44, and 64°, which were indexed as 111, 200, and 220, respectively. By using the X-ray diffraction technique, the production of the $[\text{Au}(\text{TMP})_2(\text{Cl})_2]\cdot\text{Cl}$ metal complex was verified [37]. Three peaks, which correspond to

conventional Bragg reflections (111), (200), and (220) of the face centers of the cubic lattice, represent crystalline nanoparticles. Preferential growth in the (111) direction can be seen in the sharp peak at 38. The crystallinity in the powder X-ray diffraction data was moderate. The Bragg reflections at 40°, 46°, and 67° in the XRD patterns of the $[\text{Ir}(\text{TMP})_2(\text{Cl})_2]\cdot\text{Cl}$ complex (Figure 5C) match the indexed planes of the iridium metal crystals (111), (200), and (220) [38].

Antibacterial and anticancer activities

Due to the fact that bacteria can develop a resistance to antibiotics through biochemical and morphological changes, the trimethoprim metal complexes (Standard: Ampicillin Antibacterial agent) were investigated for their antibacterial efficacy against bacteria [39]. The organisms employed in the current studies were *Pseudomonas aeruginosa* (*P. aeruginosa*), *Bacillus subtilis* (*B. subtilis*) (as gram-positive bacteria G+), *Escherichia coli* (*E. coli*), and *Staphylococcus aureus* (*S. aureus*) (as gram-negative bacteria G-). The well diffusion method was then used to assess the zone of inhibition of trimethoprim–Ru(III), trimethoprim–Au(III), and trimethoprim–Ir(III) metal complexes against G- and G+ bacteria [40]. All of the metal complexes exhibit uninhibited antibacterial activity when compared to conventional Ampicillin. When compared to the conventional antibacterial agent ampicillin, the trimethoprim–Au(III) metal combination demonstrated less effective antibacterial action.

The trimethoprim–Ru(III), trimethoprim–Au(III), and trimethoprim–Ir(III) metal complexes were evaluated for their in vitro cytotoxicity towards MCF-7 cells (human breast cancer cell line) and HepG-2 cells (human Hepatocellular carcinoma) which were obtained from VACSERA Tissue Culture Unit. Cytotoxic activity was evaluated by Viability assay for cytotoxicity assessment [41]. In order to perform the cytotoxicity assay, 1×10^4 cells per well of 96-well plates were seeded in 100 μl of growth media. After 24 hours of seeding, new medium with varying quantities of the test sample was introduced. Confluent cell monolayers were pipetted into 96-well flat-bottomed microtiter plates (Falcon, NJ, USA) using a multichannel pipette, and serial two-fold dilutions of the chemical component under test were added. Differences were considered significant at $P < 0.05$. The IC_{50} values, defined as a dose of compound that inhibits cell growth by 50%, were calculated from concentration response curves.

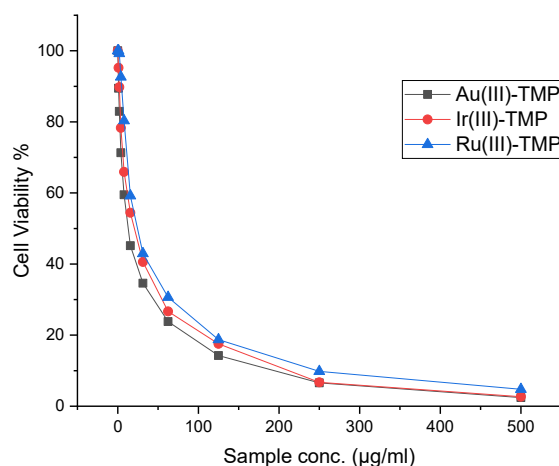


Figure 6A. Evaluation of cytotoxicity of Au ($\text{IC}_{50} = 13 \pm 0.8 \mu\text{g/mL}$), Ir ($\text{IC}_{50} = 20.6 \pm 1.6 \mu\text{g/mL}$), Ru(III)-TMP ($\text{IC}_{50} = 24.4 \pm 1.6 \mu\text{g/mL}$) complexes against HepG-2 cell line.

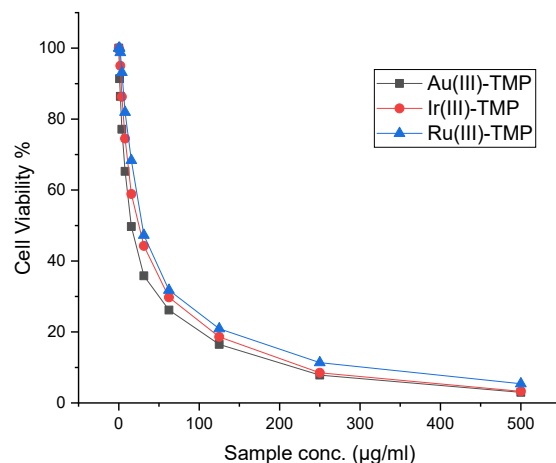


Figure 6B. Evaluation of cytotoxicity of Au ($IC_{50} = 15.5 \pm 0.9 \mu\text{g/mL}$), Ir ($IC_{50} = 25.1 \pm 1.7 \mu\text{g/mL}$), Ru(III)-TMP ($IC_{50} = 29.2 \pm 1.8 \mu\text{g/mL}$) complexes against MCF-7 cell line.

Figure 6A-B shows effect of different concentrations of tested trimethoprim complexes on two MCF-7 and HepG-2 cells after 24 incubation times. The results suggest that trimethoprim–Au(III) exhibit ($IC_{50} = 13 \pm 0.8 \mu\text{g/mL}$) and ($IC_{50} = 15.5 \pm 0.9 \mu\text{g/mL}$) effects on both HepG-2 and MCF-7 cells. The trimethoprim–Ru(III) complex exhibits cytotoxic effects on both cell lines, as ($IC_{50} = 24.4 \pm 1.6 \mu\text{g/mL}$) and ($IC_{50} = 29.2 \pm 1.8 \mu\text{g/mL}$), respectively. In case of trimethoprim–Ir(III) metal complex, the cytotoxic effect was considerably less pronounced, since calculated IC_{50} values were ($IC_{50} = 20.6 \pm 1.6 \mu\text{g/mL}$) and ($IC_{50} = 25.1 \pm 1.7 \mu\text{g/mL}$) against both HepG-2 and MCF-7 cells. Such findings could suggest that the investigated chemicals have a weaker inhibitory effect on cell proliferation or that the human breast cancer and human hepatocellular carcinoma cell lines are less susceptible to them.

CONCLUSION

This study synthesized and characterized new trimethoprim–Ru(III), trimethoprim–Au(III), and trimethoprim–Ir(III) metal octahedral complexes via elemental analysis, magnetic susceptibility, UV-Vis, FTIR, $^1\text{H-NMR}$, TGA, DSC, TEM, XRD, and SEM. The ligand performs the function of a bidentate in each compound. Evaluation of cytotoxicity of Au, Ir, Ru(III)-TMP complexes against HepG-2 cell line are ($IC_{50} = 13 \pm 0.8 \mu\text{g/mL}$), ($IC_{50} = 20.6 \pm 1.6 \mu\text{g/mL}$) and ($IC_{50} = 24.4 \pm 1.6 \mu\text{g/mL}$) and evaluation of cytotoxicity of Au, Ir, Ru(III)-TMP complexes against MCF-7 cell line are ($IC_{50} = 15.5 \pm 0.9 \mu\text{g/mL}$), ($IC_{50} = 25.1 \pm 1.7 \mu\text{g/mL}$), and ($IC_{50} = 29.2 \pm 1.8 \mu\text{g/mL}$), respectively, these metal complexes have demonstrated marginally significant cytotoxicity and antibacterial activity. It is discovered that every metal chelate is an electrolyte. These findings will undoubtedly motivate additional study on drug-metal complexes in the medical field.

ACKNOWLEDGEMENTS

Princess Nourah bint Abdulrahman University Researchers Supporting Project number (PNURSP2024R75), Princess Nourah bint Abdulrahman University, Riyadh, Saudi Arabia.

REFERENCES

1. Mashkovskii, M. *Drugs [in Russian]*, Vol. 1, Novaya Volna: Moscow; **2000**; p. 275.
2. Huang, L.; Cattamanchi, A.; Davis, J.L.; den Boon, S.; Kovacs, J.; Meshnick, S.; Miller, R.F.; Walzer, P.D.; Worodria, W.; Masur, H. International HIV-associated opportunistic pneumonias (IHOP) study, lung HIV study. HIV-associated pneumocystis pneumonia. *Proc. Am. Thorac. Soc.*, **2011**, 8, 294-300.
3. Franco, A.V.M. Recurrent urinary tract infections. *Best Practice Res. Clin. Obst. Gyn.* **2005**, 19, 861-873.
4. Ahmed, M.Z.; Habib, U. DFT studies of temperature effect on coordination chemistry of Cu(II)-trimethoprim complexes. *J. Coord. Chem.* **2018**, 71, 1102-1113.
5. Vilchêze, C.; Jacobs, W.R. The combination of sulfamethoxazole, trimethoprim, and isoniazid or rifampin is bactericidal and prevents the emergence of drug resistance in *Mycobacterium tuberculosis*. *Antimicrob. Agents and Chemother.* **2012**, 56, 5142-5148.
6. Albahadly, H.H.; Al-Haidery, N.H.; Al-Salami, B.K. Synthesis, biological activity of trimethoprim derivative and the complexes. *J. Phy.: Conf. Series* **2021**, 2063, 012014.
7. Rajapakse, C.S.K.; Martinez, A.; Naoulou, B.; Jarzecki, A.A.; Suárez, L.; Deregnacourt, C.; Sinou, V.; Schrêvel, J.; Musi, E.; Ambrosini, G.; Schwartz, G.K.; Sánchez-Delgado, R.A. Synthesis, characterization, and in vitro antimalarial and antitumor activity of new ruthenium(II) complexes of chloroquine. *Inorg. Chem.* **2009**, 48, 1122-1131.
8. Wee, H.A.; Daldini, E.; Scolaro, C.; Scopelliti, R.; Juillerat-Jeannerat, L.; Dyson, P.J. Development of organometallic ruthenium-arene anticancer drugs that resist hydrolysis. *Inorg. Chem.* **2006**, 45, 9006-9013.
9. Lebwohl, D.; Canetta, R. Clinical development of platinum complexes in cancer therapy: An historical perspective and an update. *Eur. J. Can.* **1998**, 34, 1522-1534.
10. Hartinger, C.G.; Jakupec, M.A.; Zorbas-Seifried, S.; Groessel, M.; Egger, A.; Berger, W.; Zorbas, H.; Dyson, P.J.; Keppler, B.K. KP1019, a new redox-active anticancer agent-preclinical development and results of a clinical phase I study in tumor patients. *Chem. Biodivers.* **2008**, 5, 2140-2155.
11. Sava, G.; Bergamoa, A.; Dyson, P.J. Metal-based anticancer drugs in the post-genomic era: What comes next?. *Dalton Trans.* **2011**, 40, 9069-9075.
12. Sakurai, H.; Kojima, Y.; Yoshikawa, Y.; Kawabe, K.; Yasui, H. Antidiabetic vanadium(IV) and zinc(II) complexes. *Coord. Chem. Rev.* **2002**, 226, 187-198.
13. Kiss, T.; Jakusch, T.; Hollender, D.; Dornyei, A.; Enyedy, E.A.; Pessoa, J.C.; Sakurai, H.; Sanz-Medel, A. Biospeciation of antidiabetic VO(IV) complexes. *Coord. Chem. Rev.* **2008**, 252, 1153-1162.
14. Messori, L.; Marcon, G. Gold complexes in the treatment of rheumatoid arthritis. *Metal Ions Biological Systems.* **2004**, 41, 279-304.
15. Caravan, P.; Ellison, J.J.; McMurry, T.J.; Lauffer, R.B. Gadolinium(III) chelates as MRI contrast agents: structure, dynamics, and applications. *Chem. Rev.* **1999**, 99, 2293-2352.
16. Garoufis, A.; Hadjikakou, S.K.; Hadjiliadis, N. Palladium coordination compounds as antiviral, anti-fungal, antimicrobial and anti-tumor agents. *Coord. Chem. Rev.* **2009**, 253, 1384-1397.
17. Orvig, C.; Abrams, M.J. Medicinal inorganic chemistry. *Chem. Rev.* **1999**, 99, 2201-2842.
18. Aderoju, A.; Osowole, S.M.W.; Olaoluwa, K.A. Synthesis, characterization and antimicrobial activity of some mixed drug trimethoprim-sulfamethoxazole metal drug complexes. *World Appl. Sci. J.* **2015**, 33, 336-342.
19. Almandoz, M.C.; Sancho, M.I.; Duchowicz, P.R.; Blanco, S.E. UV-Vis spectroscopic study and DFT calculation on the solvent effect of trimethoprim in neat solvents and aqueous mixtures. *Spectrochim. Acta Part A* **2014**, 129, 52-60.

20. Ajibade, P.A.; Idemudia, O.G. Synthesis, characterization, and antibacterial studies of Pd(II) and Pt(II) complexes of some diaminopyrimidine derivatives. *Bioinorg. Chem. Appl.* **2013**, *2013*, 549549.
21. Demirezen, N.; Tarınc, D.; Polat, D.; Çeşme, M.; Gölcü, A.; Tümer, M. Synthesis of trimethoprim metal complexes: Spectral, electrochemical, thermal, DNA-binding and surface morphology studies. *Spectrochim. Acta Part A* **2012**, *94*, 243-255.
22. El-Shekeil, A.; Omer, A.; Al-Aghbari, S.; Al-Shuja'a, O. Anti-cancer and anti-microbial activity studies of some complexes of trimethoprim, *J. Cancer Res. Updates* **2013**, *2*, 14-20.
23. Deacon, G.B.; Philips, R.J. Relationships between the carbon-oxygen stretching frequencies of carboxylato complexes and the type of carboxylate coordination. *Coord. Chem. Rev.* **1980**, *33*, 227-250.
24. Refat, M.S.; Al-Humaidi, J.Y.; El-Sayed, M.Y.; Hassan, R.F. In situ methanolic solvent synthesis, spectroscopic and thermogravimetric characterizations of three new transition metal complexes of trimethoprim drug. *Polish J. Chem. Technol.* **2021**, *23*, 60-67.
25. Ahmed, M.Z.; Habib, U. DFT studies of temperature effect on coordination chemistry of Cu(II)-trimethoprim complexes. *J. Coord. Chem.* **2018**, *71*, 1102-1113.
26. Guo, Z.; Sadler, P.J. Metals in medicine. *Angew Chemie Int. Ed.* **1999**, *38*, 1512-1531.
27. Alghamdi, M.T.; Alsibaai, A.A.; Shahawi, M.S.; Refat, M.S. Structural and chelation behaviors of new Ru(III), Pt(IV) and Ir(III) gatifloxacin drug complexes: Spectroscopic characterizations. *J. Mol. Struct.* **2017**, *1130*, 264-275.
28. Alibrahim, K.A.; Al-Saif, F.A.; Alghamdi, M.T.; El-Shahawi, M.S.; Moustafa, Y.M.; Refat, M.S. Synthesis, spectroscopic, thermal, antimicrobial and electrochemical characterization of some novel Ru(III), Pt(IV) and Ir(III) complexes of pipemidic acid. *RSC Adv.* **2018**, *8*, 22515-22529.
29. Alibrahim, K.A.; Al-Saif, F.A.; Alghamdi, M.T.; El-Shahawi, M.S.; Althubeiti, K.; Aljuhani, E.; Refat, M.S. Spectroscopic, molecular structural, thermal, biological and voltammetric characterization of Ru³⁺, Pt⁴⁺ and Ir³⁺ complexes of lomefloxacin drug. *Lat. Am. J. Pharm.* **2019**, *38*, 1077-1090.
30. Alosaimi, E.H.; Alsibaai, A.A.; El-Shahawi, M.S.; Refat, M.S. Synthesis, physicochemical and thermal analyses of Ru(III), Pt(IV) and Ir(III) complexes with NO bidentate Schiff base ligand. *Russ. J. Phys. Chem. A* **2018**, *92*, 2227-2236.
31. Alosaimi, E.H.; Alsibaai, A.A.; El-Shahawi, M.S.; Refat, M.S. Spectrochemical, thermal, and kinetic thermodynamic characterizations of 3-[(2-hydroxy-phenylimino)-methyl]-benzene-1,2-diol Schiff base ruthenium(III), platinum(IV) and iridium(III) complexes in nano scale size. *J. Comp. Theo. Nanosci.* **2017**, *14*, 3747-3757.
32. Lever, A.B. *Inorganic Electronic Spectroscopy*, Elsevier: Amsterdam; **1968**.
33. Figgis, B.N. *Introduction to Ligand Field Theory*, 1st ed., Interscience Publishers: New York; **1967**; p. 287.
34. Bergh, J.J.; Breytenbach, J.C.; Wessels, P.L. Degradation of trimethoprim. *J. Pharm. Sci.* **1989**, *78*, 348-350.
35. Fernandes, N.S.; Carvalho Filho, M.A.S.; Mendes, R.A.; Ionashiro, M. Thermal decomposition of some chemotherapeutic substances. *J. Braz. Chem. Soc.* **1999**, *10*, 459-462.
36. González-Huerta, R.G.; González-Cruz, R.; Citalán-Cigarroa, S.; Montero-Ocampo, C.; Chavez-Carvayar, J.; Solorza-Feria, O. Development and electrochemical studies of ruthenium nanoparticles as cathode in a PEMFC. *J. New Mat. Electrochem. Systems* **2005**, *8*, 15-23.
37. Sneha, K.; Sathishkumar, M.; Kim, S.; Yun, Y.S. Counter ions and temperature incorporated tailoring of biogenic gold nanoparticles. *Process Biochem.* **2010**, *45*, 1450-1458.
38. Yan, X.; Ai, T.; Su, X.; Wang, Z.; Sun, G.; Zhao, P. Synthesis and thermal decomposition mechanism study of a novel iridium precursor. *MATEC Web of Conferences* **2016**, *43*, 01002. doi:10.1051/mateconf/20164301002.

39. Mihorianu, M.; Heiko Franz, M.; Jones, P.G.; Kelter, M.F.G.; Fiebig, H.H.; Tamm, M.; Neda, I. N-Heterocyclic carbenes (NHC) derived from imidazo [1,5-a] pyridines related to natural products: synthesis, structure and potential biological activity of some corresponding gold(I) and silver(I) complexes. *Appl. Organometal. Chem.* **2016**, 30, 581-589.
40. Patel, M.N.; Parmar, P.A.; Gandhi, D.S. Third generation fluoroquinolones antibacterial drug based mixed-ligand Cu(II) complexes: structure, antibacterial activity, superoxide dismutase activity and DNA-interaction approach. *J. Enzyme Inhib. Med. Chem.* **2011**, 26, 188-197.
41. Gomha, S.M.; Riyadh, S.M.; Mahmmod, E.A.; Elaasser, M.M. Synthesis and anticancer activities of thiazoles, 1,3-thiazines, and thiazolidine using chitosan-grafted-poly(vinylpyridine) as basic catalyst. *Heterocycles* **2015**, 91, 1227-1243.